Stress Distribution Around Osseointegrated Implants With Different Internal-Cone Connections: Photoelastic and Finite Element Analysis

Lilian Costa Anami, DDS, MSc[1]*
Júlia Magalhães da Costa Lima, DDS, PhD[1]
Fernando Eidi Takahashi, DDS, PhD[2]
Maximiliano Piero Neisser, DDS, PhD[2]
Pedro Yoshito Noritomi, PhD[3]
Marco Antonio Bottino, DDS, PhD[2]

The goal of this study was to evaluate the distribution of stresses generated around implants with different internal-cone abutments by photoelastic (PA) and finite element analysis (FEA). For FEA, implant and abutments with different internal-cone connections (H- hexagonal and S- solid) were scanned, 3D meshes were modeled and objects were loaded with computer software. Trabecular and cortical bones and photoelastic resin blocks were simulated. The PA was performed with photoelastic resin blocks where implants were included and different abutments were bolted. Specimens were observed in the circular polariscope with the application device attached, where loads were applied on same conditions as FEA. FEA images showed very similar stress distribution between two models with different abutments. Differences were observed between stress distribution in bone and resin blocks; PA images resembled those obtained on resin block FEA. PA images were also quantitatively analyzed by comparing the values assigned to fringes. It was observed that S abutment distributes loads more evenly to bone adjacent to an implant when compared to H abutment, for both analysis methods used. It was observed that the PA has generated very similar results to those obtained in FEA with the resin block.

Key Words: internal-cone connections, finite element analysis, photoelasticity

Downloaded from http://meridian.allenpress.com/joi/article-pdf/41/2/155/2035673/aaid-joi-d-12-00260.pdf by guest on 17 April 2024

INTRODUCTION

Since the 1980s, dentists and patients have been increasing the demands for aesthetics.[1,2] The development of osseointegrated implants[2] brought a wide range of options for functional and aesthetic teeth replacement. Bone resorption is known to be one of the major complications in implant treatment.[3] Research has shown that some bone loss around implants can be considered clinically acceptable (an average of 0.9 mm in the first year and 0.1 mm in the following years).[4,5] A crucial factor that affects the outcome of implant treatment is the way occlusal forces are transferred to the bone-implant interface. This interface must tolerate occlusal forces without adverse tissue response.[6] According to some authors,[7–10] it is essential to have an implant designed to functionally distribute occlusal loads to peri-implant bone at physiological levels.

The geometric configuration of each component of bone/implant/abutment complex influences the dental implant's biomechanical behavior.[11] According to Çehreli et al,[6] the influence of implant design and implant-abutment interface on marginal bone reactions is still unclear.

Internal connections stand out when compared to external ones because they have less loosening and loss of screw, better external overloads absorption,[12] and more homogeneous stresses distribution around implants.[13] According to Hermann et al,[14] one-piece titanium implants show superior stability when compared to two-piece implants with internal connection due to greater depth of retention and increasing the contact area between abutment and implant walls.

Other authors[15,16] found further promising evidence for using internal-cone connections. After clinically evaluated implants that have been in function for 10 years, Morris et al[16] have encountered no bone resorption; in some cases, they found a slight bone growth on the implant platform. These results may be associated with the fact that this connection is stable (does not allow micro-movements between abutment and implant) and presents no interface discontinuity between components. This type of connection tends to improve the implant biomechanical behavior[17] but has the impossibility of

[1] Graduate Program in Restorative Dentistry, Prosthetic Dentistry Unit, Institute of Science and Technology - São José dos Campos, Univ Estadual Paulista (UNESP), Brazil.
[2] Department of Dental Materials and Prosthodontics, Institute of Science and Technology - São José dos Campos, Univ Estadual Paulista (UNESP), São Paulo, Brazil.
[3] Centro de Tecnologia da Informação Renato Archer, Campinas, São Paulo, Brazil.
* *Corresponding author,* e-mail: lianami@gmail.com
DOI: 10.1563/AAID-JOI-D-12-00260

repetition as an inherent problem. Without any indexing feature, it is not possible to safe transfer the exact location of the abutment.[18]

The development of designs played an important hole in the internal-cone taper evolution. Today, there are commercially internal-cone abutment models that contains—in addition to the "Morse cone"—stabilizing elements such as locking screws and antirotational hexagon. The presence of two stabilizing elements has resulted in a strong, stable, and predictable connection. The new design allows the achievement of a great connection. Although, according Binon,[18] the combination of the cone with these elements mischaracterizes the connection as a real Morse taper.

In addition to the internal-cone and the locking screws, the two-piece hexagon abutments have an internal hexagon to allow for precision repositioning of the components during the lab and clinical steps.

The main methods of investigation and biomechanical analysis of prosthetic components are: finite elements analysis (FEA), photoelasticity, strain-gauge, and evaluation of bond resistance between implant and bone tissue through shearing, traction, and compression tests.[19] According to Turcio et al,[19] a photoelastic analysis should be combined with the FEA, as the first provides a more qualitative result of the stress distribution, whereas the finite element method provides more detailed information of the complete state of the tensions.[20]

Therefore, the aim of this study was to test the hypothesis that the prosthetic component does not influence the load transferred to the surrounding bone and that the results obtained by photoelastic method and FEA are comparable.

Materials and Methods

FEA

Initially, the properties of an epoxy resin block (Araldite BR GY 279 and hardener HY 2963 BR, Araltec Produtos Químicos Ltda, Sao Paulo, SP, Brazil) with approximate dimensions $38 \times 10 \times 7$ mm and mass 2.93 g used for the photoelastic analysis were characterized by impulse excitation of vibration. Specimens of this material present specific mechanical resonant frequencies determined by the elastic modulus, mass, and geometry.

The flexural and torsional resonant vibration was measured using Sonelastic (ATCP Engenharia Física, São Carlos, SP, Brazil). The elastic modulus was determined using the resonant frequency in the flexural mode. The shear modulus was obtained using torsional mode. The Poisson's ratio was then calculated from those data.

Cortical screw (Master Ar Morse Porous 3.75×13 mm) and abutments (Hexagonal Micro-Unit Morse taper and Solid Micro-Unit Morse taper abutments, Conexão Sistemas de Prótese Ltda, Arujá, SP, Brasil) (Figure 1) were scanned by a computed micro tomography X-ray scanner (SkyScan 1172, SkyScan, Kontich, Belgium) (pixel size: 14.97 μm, voltage: 100 kV, current: 100 μA, rotation step: 0.40 deg, metal artifact: Al + Cu).

Images obtained were converted to Digital Imaging Communications in Medicine (DICOM) format compatible with InVesalius 3.0 reconstruction software (CTI Renato Archer, Sao Paulo, SP, Brazil). This software creates stacks of micro-CT images and generates 3D images from scanned objects in STL format (stereolithography, standard format for fast prototyping).

STL images were then sent to CAD software Rhinoceros 4.0 (Robert McNeel & Associates, Seattle, Wash) to generate the 3D geometry of the objects. The 3D models promote results with more information and clinically relevant data.[21] In this step, we chose to perform the simplification of the drawing, replacing all helical threads by rings and ignoring the surface thread where the abutments would be bolted to the prosthetic piece. This happened with the objective to reduce the time spent refining the mesh and avoid wastage of elements during FEA. These simplifications do not commit this type of analysis.[22]

Geometry generated by a CAD program was imported to FEMAP software (Finite Element Modeling and Postprocessing, version 10.10, Siemens PLM Software, Köln, Germany), which had performed a preprocessing phase. In this stage, material properties were assigned (Table 1).

To allow use of a larger number of elements in the analysis and assuming a symmetrical distribution of the strains under axial load, a quarter of the assembly was digitally sectioned and used for the analysis. All materials were considered static, linear, homogeneous, and isotropic.

The base of the block was fixed to prevent movements in all directions (x, y, z). It was assumed a perfect contact for all the interfaces by assigning "bonded" contact-type between the screw surfaces and "not bonded" for the other contact areas. The bonded contact-type is assigned when a perfect union between surfaces is desired, preventing the slip of one over the other or the separation of both. There was no surface penetration for the contacts.

The loading was standardized to allow the comparison of the data from FEA and photoelastic method. A 14 kgf force with an 8 mm diameter tip was applied in the center of the top surface of the abutment. There was no preloading. Assigning the bonded contact-type simulated part of the torque effect for the pretension of the bolts.

The cortical screw was composed of 42 147 elements. The number of elements for the solid abutment was 15 268, while the hexagonal abutment and its retaining screw totaled 22 818 elements. A total of 90 661 elements were used to replicate the resin block and solid abutment, 98 211 for resin block and hexagonal abutment, 95 101 for bone block and solid abutment, and 102 651 to bone block and hexagonal abutment.

All pre-processing information was transformed into numerical data and sent to NEiNastran processing computational software (version 9.2, Finite Element Analysis and Simulation Software Noran Engineering Inc, Westminster, Calif) for the static mechanical analysis. The postprocessing phase was done in FEMAP software.

Photoelastic analysis

The resin block for the photoelastic analysis was produced by CO_2 laser polymerization of 0.1 mm increments of nylon DuraForm PA (PA12 based) powder guided by the .STL file sent to the additive manufacturing machine (Sinterstation 2000, 3D Systems, Valencia, Calif).

The prototyped block was placed in a bench drilling

Downloaded from http://meridian.allenpress.com/joi/article-pdf/41/2/155/2035673/aaid-joi-d-12-00260.pdf by guest on 17 April 2024

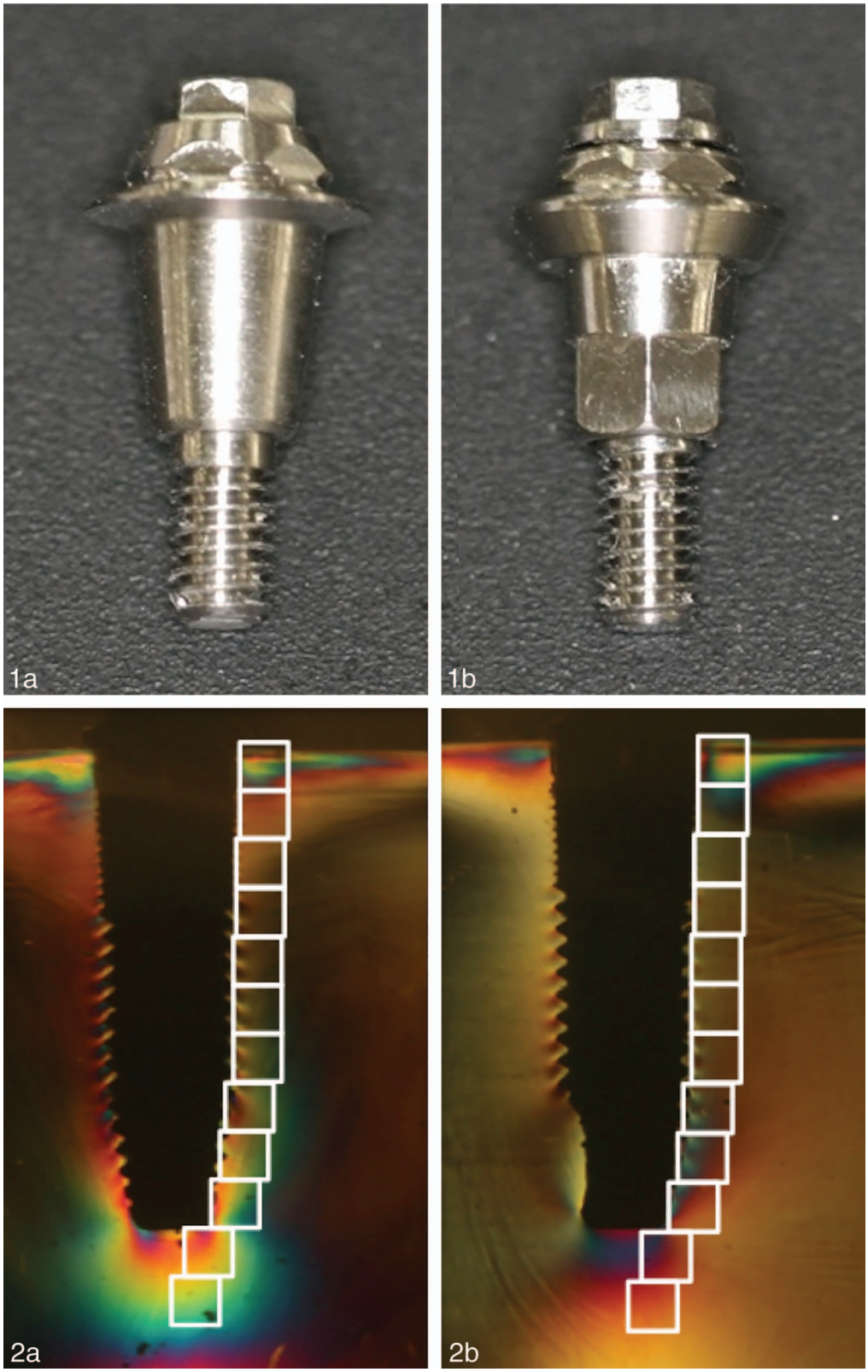

Figures 1 and 2. Figure 1. (a) Hexagonal abutment. (b) Solid abutment. **Figure 2.** Close-up view of the points of analysis for (a) hexagonal abutment and (b) solid abutment systems.

Downloaded from http://meridian.allenpress.com/joi/article-pdf/41/2/155/2035673/aaid-joi-d-12-00260.pdf by guest on 17 April 2024

TABLE 1

Mechanical properties of biological structures and titanium used: elasticity modulus (E - GPa) and Poisson's ratio (ν)

Structure	Young's Modulus (GPa)	Poisson Ratio (ν)	Reference
Photoelastic resin	2.07	0.41	tested
Cortical bone	13.7	0.3	Rubo and Souza[23]
Trabecular D2 bone	7.9	0.3	
Pure commercially titanium	110.0	0.35	

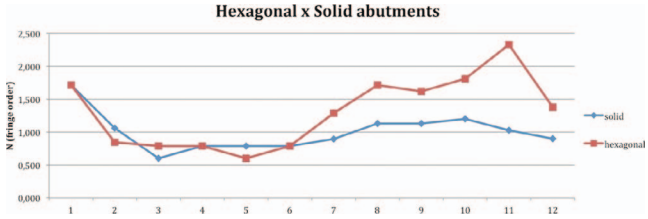

FIGURE 3. Graphic with observation points values × mean of fringe order (N) for hexagonal and solid abutments on photoelastic analysis.

(Diplomat M-3, Deb'maq do Brazil Ltda, Camanducaia, MG, Brazil) for enlargement of the perforation using high-speed steel drills.

Initially, a Hexagonal Micro-Unit abutment (Conexão) was attached on the implant (Morse Porous Ar Master 3.75 × 13 mm, Conexão) and torqued to 20 Ncm. The square transfer for Micro-Unit (Conexão) was positioned and attached to the abutment. The set was inserted into the block until the cervical portion of the implant was flush to the block top surface. The same steps were performed for the solid Micro-Unit abutment (Conexão)

Impressions were taken by the open tray technique using a white rubber silicone (ABCol, Sao Caetano do Sul, SP, Brazil).

With a clamp, the abutments were fastened over the implants, and 20 Ncm torque was checked for both abutments. Then, the implant/abutment joint was fitted, bolted to the transfers, and positioned within the molds. The molds were filled with epoxy resin (GY 279 BR and HY 2963 BR, Araltec) and let set for 72 hours for complete polymerization.

The polymerized resin and implant contact simulated the full osseointegration.[24] A dark field circular polariscope mounted with a light source (Photoflood n2, GE General Electric, Sao Paulo, SP, Brazil), a light filter diffuser, polarizer, and analyzer plates, two quarter-wave plates (Eikonal Optical Instruments, Sao Paulo, SP, Brazil), and a camera (Canon EOS Rebel XT, Canon Inc, Tokyo, Japan) coupled to a load application device composed by a support of 1 kg, 13 kg boards, and a 8 mm diameter flat-tipped applicator, attached to the parallelometer (Bio Art Dental Equipment, Sao Carlos, SP, Brazil), totaling 14 kg.

A photoelastic model was inserted in a virgin acrylic container containing mineral oil (Nativita Indústria e Comércio, Juiz de Fora, MG, Brazil) to reduce surface refractive and facilitate the photoelastic observation.[25] To confirm the absence of residual tensions, models were initially observed with absence of charge in the field of circular polariscope.[25,26]

It was necessary to release the tension, and the models were placed in an oven (Orion 502, Fanem, Sao Paulo, SP, Brazil) at 37°C for 15 minutes. This protocol proved sufficient to relieve tension and was secure to the material structure, being below the resin thermal decomposition temperature given by the manufacturer (200°C).

After loading the parallelometer, tensions observed on the polariscope were recorded by the digital camera. Images obtained in photoelasticity were transferred to a computer and evaluated two ways: qualitatively, following preset parameters established by other studies[24,27,28] in which the higher the proximity between the fringes, higher stress concentration, and the greater the number of order fringe (or the number of fringes), the greater the magnitude of tension; and quantitatively, by comparing the fringe values according to the fringe color proposed by the American Society for Testing and Materials.[29]

For quantitative analysis, the digital images were imported to PowerPoint 2008 software for Mac (Microsoft, Redmond, Wash), and a series of 12 equal dimensions squares was added as preset points of analysis.

A descriptive analysis was done for FEA results by visual observation of graphic images of the displacement and maximum, and Von Mises stress occurred in the structures of the models.

For better comparison of data between blocks, strains resulting values were analyzed in three points on each block—all on the left side of the contact area with the implant—as follows: CE – implant cervical; BE – 8.5 mm below the implant cervical, and AE – implant apical.

RESULTS

Photoelastic analysis

The hexagonal abutment showed high fringe order values around CE and AE of the cortical screw, suggesting higher stress in these areas. At CE, very close fringes were also observed around the cortical screw, suggesting a concentration of stress. The solid abutment model showed low fringe values at AE. However, the fringes were very close and with a high value at the cortical screw CE area, suggesting high magnitude and concentrated stress. When comparing the two abutments, the hexagonal one showed higher fringe values overall and at specifics points as well.

Figure 2 shows 12 points for quantitative analysis for each model. Two calibrated operators performed the evaluation. The reproducibility error for the 2 calibrated operators was determined by Dahlberg test. The difference between operators was 0.695 N for the hexagonal and 0.688 N for the solid abutment model. These values are considered low, reflecting a great consistency between operators.

Figure 3 shows a graphic of analysis points × mean between operator's results. It allowed a point-by-point analysis.

The solid abutment showed results more homogeneously distributed (Figure 4b), while the hexagonal had stress concentrated at CE and AE (Figure 4a).

Downloaded from http://meridian.allenpress.com/joi/article-pdf/41/2/155/2035673/aaid-joi-d-12-00260.pdf by guest on 17 April 2024

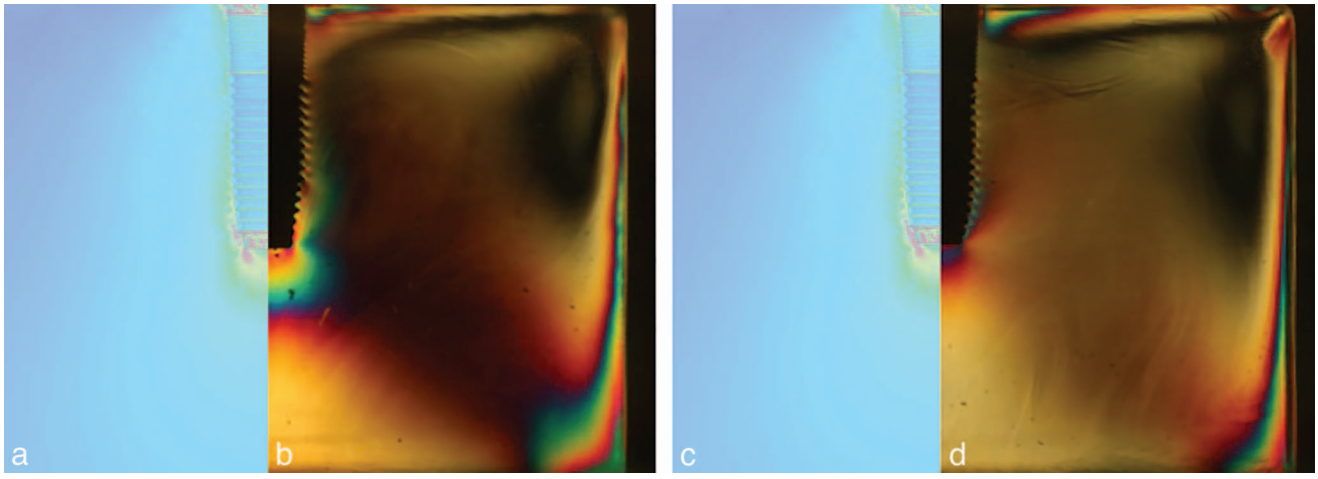

Figure 4. Comparison of results after 14 kgf load on hexagonal abutment model at (a) FEA and (b) photoelastic analysis, and the solid abutment model for (c) FEA and (d) photoelastic analysis.

FEA

The hexagonal abutment/resin block system showed a low displacement, with the abutment/cortical screw components behaving as a single unit (Figure 5a).

The von Mises stress distribution through the resin was fairly uniform, with a slightly concentration of the top edge around the cortical screw. The cortical screw showed higher stress concentration at the cervical area, distributed all over the contact surface. A second stress concentration point was located on the first two threads of the small thread (top area) and large thread (center area). Except for these points, the stress was homogeneously distributed through the implant body.

The solid abutment/resin block system showed a displacement pattern similar to the previous model (Figure 5c).

There was a slightly stress concentration in the top area at the contact surface between the implant and the block. The FEA showed similar behavior to the hexagonal/resin block system.

Figure 4 compares the FEA and photoelastic analysis for both systems. Although the photoelastic analysis showed differences in stress concentration between the two systems, the FEA showed, through a clear view, a similar and homogeneous stress distribution for both systems.

The displacement on the hexagonal abutment/bone block system was similar to the resin block one (Figure 5b). The cortical bone absorbed almost all von Mises stress, and the trabecular bone was only slightly requested.

The solid abutment/bone block system also behaved similarly to the resin block system and had lower values when compared to the hexagonal abutment/bone block (Figure 5d). There was a slight difference in the thickness of the fringes with higher displacement values from the cortical to the trabecular bone and from the solid abutment to the cortical screw. This model showed similar stress distribution between the cortical and trabecular bone (however, with lower values). Looking from outside, the cortical screw showed almost all stress concentrated at the cervical edge, right at the cortical bone level. There were higher stress values in the contact area with the cortical bone. When observing the trabecular bone, the first thread of the large thread could be seen as a stress concentration point.

The von Mises stress for all the chosen points are shown in Table 2.

Discussion

Many different osseointegrated implants and components designs are currently available in the market, giving dentists a wide variety of options for oral rehabilitation treatment. For implants with an internal connection, the conical abutment-implant (Morse taper) can be distinguished by its bulkiness,[3,15–17] with a large contact area between the implant and the abutment walls, providing a more uniform stress distribution. The great attrition between these two surfaces ensures stability and retention for the system.

The components used for dental implants are designed to support and transmit functional forces to surrounding bone within physiological limits.[7,8] The geometry of these components influences the biomechanical behavior of the overall system.[11]

Solid and hexagonal abutments are externally similar, with a small difference in the geometry. The solid one has a screw added to internal-cone that, according to Hermann et al[14] and Morris et al,[16] works as a stable connection, with great biomechanical behavior and no gap between components.

The presence of an hexagon on the apical half of the internal-cone given the hexagonal abutment enables more reliable position transfer,[18] providing a more stable connection that creates better resistance against rotational movements for single crowns.[3]

Similar to Çehreli et al,[30] this study obtained resembling characteristics of stress distribution under vertical loading for abutments with different internal-cone connections. The photoelastic analysis showed significant concentration of stress in the cervical and apical areas for the hexagonal abutment model, with symmetrical distribution. For the solid abutment model, it showed asymmetrical stress concentration only at the

Downloaded from http://meridian.allenpress.com/joi/article-pdf/41/2/155/2035673/aaid-joi-d-12-00260.pdf by guest on 17 April 2024

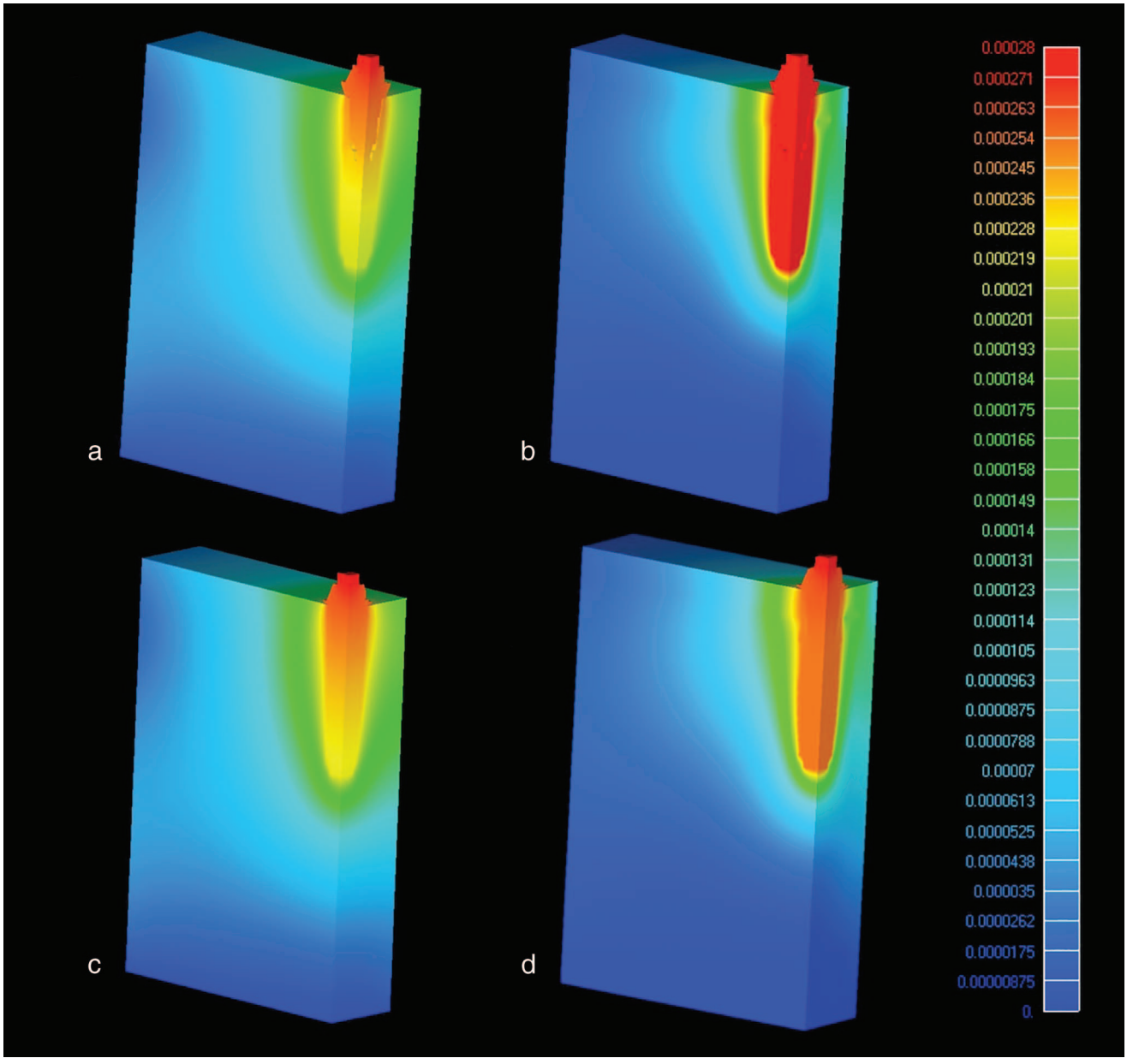

Figure 5. Comparison of FEA total displacement, fixed scale to models (a) resin/hexagonal abutment, (b) bone/hexagonal abutment, (c) resin/holid abutment and (d) bone/holid abutment.

Table 2

von Mises stress on chosen points for hexagonal and solid abutments*

		von Mises Stress on Points (MPa)		
Block	Abutment	CE	BE	AE
Resin	Hexagonal	0.210	0.060	0.171
	Solid	0.170	0.060	0.153
Bone	Hexagonal	0.310	0.000642	0.002
	Solid	0.595	0.000537	0.002

*CE indicates implant cervical; BE, 8.5 mm below the implant cervical; AE, implant apical.

neck, followed by uniform distribution in the rest of the abutment. The asymmetric distribution of stress in the solid abutment model can be associated with the cortical screw rotation that happened during fabrication of the models. Thus, one cut-threads of the cortical screw in the solid abutment specimen was perpendicular to the axis of tension observation. It is possible to observe, according to the graph in Figure 3, that the stress lines of the two models start separating themselves at the seventh spot—an area that corresponds to the beginning of the threads. This might have masked the real stress distribution in this area of the model. However, due to the number that this geometry is found in the cortical screw used in this study (three cut-threads), the distribution at 120°

Downloaded from http://meridian.allenpress.com/joi/article-pdf/41/2/155/2035673/aaid-joi-d-12-00260.pdf by guest on 17 April 2024

makes difficult identical positioning among the different models, since this screw is inserted into the block when it made its prototyped position transferred to the mold that had the photoelastic resin.

For the hexagonal abutment in the FEA, there was significant stress concentration in the neck where bone contacted the implant in the cervical area of the cortical screw and where the abutment contacted the cortical screw. In both cases, this concentration may be associated with possible finite element mesh areas of premature contact.

Still on the same model, there was stress concentration inside the cortical screw near the contact with the abutment. There was also stress concentration in the abutment in the same area. This shows a great stress transfer from the cortical screw to the abutment.

The solid abutment/bone model showed a more homogeneous stress distribution, with no stress concentration from premature contact. Externally, there was a higher stress concentration in the cervical area of the cortical screw, while there was a homogeneous distribution all over the contact area with the solid abutment. This fact can be associated to the larger wedge effect of this geometry, creating a higher demand in the exterior of the solid abutment, mainly in the neck.

With respect to solid abutment, this study observed that the abutment to cortical screw stress distribution occurs solely by the abutment cone, with no request from the retaining screw region.

Future studies aimed at assessing the actual need for retaining screws should be made in these cases since if no extrusive forces on the abutment or the friction from the walls outside and inside the abutment screw in the cone region is sufficient to retain the abutment position, the use of these may be unnecessary. In this case, and according to Merz et al,[22] this tapered design of the interface that maintains a high normal pressure contact zone given by frictional forces could be enough to hold a stable the prosthetic abutment in position.

With respect to the bone block, stress distribution has proved to be similar in hexagonal and solid abutments, with no important differences in this regard.

The way the chewing loads transfer to the implant surrounding bone is a crucial biomechanical factor for osseointegration and fundamental to the success of the rehabilitation treatment.[6] For this reason, photoelasticity was chosen since this method makes it possible to visualize the stress distribution and the magnitude of the refractive index on a birefringent material. The photoelastic fringes represent tension and compression stresses.

There are a great number of photoelastic materials commercially available, each with different mechanical properties. According to Sirohi,[31] the chosen material must have mechanical properties similar to the bone structure. However, all photoelastic materials are homogeneous after polymerized, and the bone tissue is a heterogeneous structure. While the photoelastic resin is a homogeneous and isotropic material, the implants are placed in a bone characterized by its heterogeneity and anisotropy.[32] The elasticity modulus ranges from 13.7 GPa for cortical bone and 7.3 GPa for D2-type trabecular bone,[23] and the photoelastic resin has elasticity modulus of 2.07 GPa.

In 1962, Frocht[33] wrote that photoelastic analysis was indicated for situations where the FEA was not possible. Currently, advances in the technology have changed this situation. The results of this study corroborate with other authors[6,27,32,34] about some limitations in the technique. In addition to the disadvantage of getting superimposed results on a quasi-tridimensional analysis,[27] the photoelasticity has no physical resolution to differentiate stress gradient around the threads[6] and cannot reproduces heterogeneous materials.

The FEA is a computational method in which an approximate model simulates a real structure from mathematical calculations, the expected behavior for the structure under the given conditions, and mechanical properties of the materials. Thus, if a material's mechanical properties can be calculated, its behavior can be simulated by this method.

The FEA provides von Mises stress and total displacement results as one of its possible results. Similar to photoelastic analysis, the von Mises stress represents two states of stress: tension and compression.

There was a great reciprocity in the results of von Mises stress for the photoelastic method and FEA for the resin block. This can be interpreted as a positive correlation to the use of photoelasticity for simulation of laboratory conditions.

The resin blocks showed higher values of displacement than did the bone blocks (Table 2). While the CE and AE values were similar for the resin blocks, there was a great difference between them on the bone blocks. This can possibly be related to the fact that the elastic modulus and the material composition are different. The resin absorbs stress more evenly, while in bone blocks, most of the stress is absorbed by the cortical layer with only a small portion transmitted to the trabecular bone.

With increased use of photoelasticity as a methodology for inhomogeneous structures analyses, it would be interesting to note development of resins with different compositions, allowing densities similar to cortical and trabecular bone. The addition of different amounts of silanized glass filler particles could possibly be the solution, if the addition does not change the translucency of the material needed for photoelastic analysis. If these resins were developed, the next step would be to test the results by ensuring the similarity between the simulated and original materials and then validating the method as a complementary technique to FEA.

In both analyses, we adopted a centered load because lateral ones are more demanding for the surrounding bone,[35] and the excess of this type of loading can lead to crater-like bone defects.[36] Although the centered loads would simulate a "perfect" restoration from a biomechanical point of view,[37] this is not always the reality. We agree, however, that the direction of loading may result in other stresses,[38] and this is one limitation of the present work.

Conclusion

It can be concluded that solid abutment load transferring to the adjacent bone of implant was more homogeneous than for the hexagonal abutment, for both analyses methods used.

Downloaded from http://meridian.allenpress.com/joi/article-pdf/41/2/155/2035673/aaid-joi-d-12-00260.pdf by guest on 17 April 2024

The results of photoelastic analysis were very similar to those obtained for FEA in the resin block systems.

The analysis by FEA showed significant differences of the distribution of stresses around the implants between the resin and bone blocks.

Abbreviations

AE: implant apical
BE: 8.5 mm below the implant cervical
CAD: computer-aided design
CE: implant cervical
FEA: finite element analysis
FEMAP: finite element modeling and postprocessing
PA: photoelastic analysis
STL: stereolithography

Acknowledgments

This project was supported by CAPES (Brazil). The authors gratefully acknowledge CTI Renato Archer (Campinas, SP, Brazil) for their skillful technical assistance with the FEA surveys.

References

1. Brisman AS. Esthetics: a comparison of dentists' and patients' concepts. *J Am Dent Assoc*. 1980;100:345–352.

2. Branemark P-I, Zarb GA, Albrektsson T. *Tissue-Integrated Prostheses: Osseointegration in Clinical Dentistry*. Chicago: Quintessence; 1985.

3. Arvidson K, Bystedt H, Frykholm A, van Konow L, Lothingius E. Five-years prospective follow-up report of the Astra Tech dental implant system in the treatment of edentulous mandible. *Clin Oral Impl Res*. 1998;9:225–234.

4. Adell R, Lekholm U, Rockler B, Branemark P-I. A 15-year study of osseointegrated implants in the treatment of the edentulous jaw. *Int J Oral Surg*. 1981;10:387–416.

5. Goodacre CJ, Bernal G, Rungcharassaeng K, Kan JYK. Clinical complications with implants and implant prostheses. *J Prosthet Dent*. 2003; 90:121–132.

6. Çehreli MC, Duyk J, De Cooman M, Puers R, Naert I. Implant design and interface force transfer. A photoelastic and strain-gauge analysis. *Clin Oral Impl Res*. 2004;15:249–257.

7. Brunski JB. Biomaterials and biomechanics in dental implant design. *Int J Oral Maxillofac Implants*. 1988;3:85–97.

8. Frost HM. Skeletal structural adaptations to mechanical usage (SATMU): 1. Redefining Wolff's law: the bone modeling problem. *Anat Rec*. 1990;226:403–413.

9. Frost HM. Wolff's Law and bone' structural adaptations to mechanical usage: an overview for clinicians. *Angle Orthod*. 1994;64:175–188.

10. Pesqueira A, Goiato M, Gennari-Filho H, Monteiro D, dos Santos D, Haddad M, Pellizzer E. The use of stress analysis methods to evaluate the biomechanics of oral rehabilitation with implants. *J Oral Implantol*. 2014;40: 217–228.

11. Skalak R. Biomechanical considerations in osseointegrated prostheses. *J Prosthet Dent*. 1983;49:843–848.

12. Norton MR. An in vitro evaluation of the strength of an internal conical interface compared to a butt joint interface in implant design. *Clin Oral Impl Res*. 1997;8:290–298.

13. Hansson S. A conical implant-abutment interface at the level of the marginal bone improves the distribution of stresses in the supporting bone: an axisymmetric finite element analysis. *Clin Oral Impl Res*. 2003;14:286–293.

14. Hermann J, Buser D, Schoolfield JD, Cochran DL. Biologic width around one and two-piece titanium implants: a histometric evaluation of unloaded nonsubmerged and submerged implants in the canine mandible. *Clin Oral Impl Res*. 2001;12:559–571.

15. Chou C, Morris HF, Walker L, DesRosiers D. AICRG, part II: crestal bone loss associated with the ankylos implant: loading to 36 months. *J Oral Implantol*. 2004;30:134–143.

16. Morris H, Ochi S, Crum P, Orenstein IH, Winkler S. AICRG, part I: a 6-year multicentered, multidisciplinary clinical study of a new and innovative implant design. *J Oral Implantol*. 2004;30:125–133.

17. İplikçioğlu H, Akça K, Çehreli MC, Sahin S. Comparison of non-linear finite element stress analysis with in vitro strain gauge measurements on a Morse taper implant. *Int J Oral Maxillofac Implants*. 2008;18:258–265.

18. Binon PP. Implants and components: entering the new millennium. *Int J Oral Maxillofac Implants*. 2000;15:76–95.

19. Turcio KHM, Goiato MC, Gennari Filho H, Santos DM. Photoelastic analysis of stress distribution in oral rehabilitation. *J Craniofac Surg*. 2009;20: 471–474.

20. Farah JW, Craig RG. Reflection of photoelastic stress analysis of a dental bridge. *J Dent Res*. 1971;50:1253–1259.

21. Yamanishi Y, Yamaguchi S, Iamazato S, Nakano T, Yatani H. Influences of implant neck design and implant-abutment joint type on peri-implant bone stress and abutment micromovement: three-dimensional finite element analysis. *Dent Mater*. 2012;28:1126–1133.

22. Merz BR, Hunenbart S, Belser UC. Mechanics of the implant-abutment connection: an 8-degree taper compared to a butt joint connection. *Int J Oral Maxillofac Implants*. 2000;15:519–526.

23. Rubo JH, Souza EAC. Computational methods applied to bioengeneering: solution of load problems in implant prosthesis. *J Appl Oral Sci*. 2001;9:97–103.

24. French DMD, Bowles CQ, Parham PL, Eick JD, Killoy WJ, Cobb CM. Comparison of peri-implant stresses transmitted by four commercially available osseointegrated implants. *Int J Periodontics Restor Dent*. 1989;9:221–230.

25. Frederick DR, Caputo AA. Effects of overdenture retention designs and implant orientations on load transfer characteristics. *J Prosthet Dent*. 1996;78:624–632.

26. Ueda C, Markarian RA, Sendyk CL, Laganá DC. Photoelastic analysis of stress distribution on parallel and angled implants after installation of fixed prostheses. *Braz Oral Res*. 2004;18:45–52.

27. Caputo AA, Standlee JP. *Biomechanics in Clinical Dentistry*. Chicago: Ouintessence Publ Co; 1987.

28. Markarian RA, Ueda C, Sendyk CL, Laganá DC, Souza RM. Stress distribution after installation of fixed frameworks with marginal gaps over angled and parallel implants: a photoelastic analysis. *J Prosthodont*. 2007:16: 117–122.

29. American Society for Testing and Materials. *D4093-95 reapproved 2001: Standard Test Method for Photoelastic Measurements of Birefringence and Residual Strains in Transparent or Translucent Plastic Materials*. West Conshohocken, Pa: ASTM International; 2001.

30. Çehreli MC, Akça K, İplikçioğlu H. Force transmission of one- and two-piece Morse-taper oral implants: a nonlinear finite element analysis. *Clin Oral Impl Res*. 2004;15:481–489.

31. Sirohi RS. *Optical Methods of Measurement. Wholefield Techniques*. New York: Taylor & Francis; 2008.

32. Yu P-S, Yoo Y-S, Kim K-W. A photoelastic study of the stress distribution on canine retraction by segmented TMA T-loop spring. *Korea J Orthod*. 2001;31:199–207.

33. Frocht MM. *Photoelasticity*. New York: Wiley; 1962.

34. Mahler DB, Peyton FA. Photoelasticity as a research technique for analyzing stresses in dental structures. *J Dent Res*. 1955;34:831–838.

35. Kitamura E, Stegaroiu R, Nomura S, Miyakawa O. Influence of marginal bone resorption on stress around an implant—a three-dimensional finite element analysis. *J Oral Rehabil*. 2005;32:279–286.

36. Duyck J, Ronold HJ, Oosterwyck HV, Naert I, Sloten JV, Ellingsen JE. The influence of static and dynamics loading on marginal bone reactions around osseointegrated implants: an animal experimental study. *Clin Oral Impl Res*. 2011;12:207–218.

37. Bernardes SR, de Araújo CA, Neto AJ, Simamoto Júnior P, das Neves FD, Photoelastic analysis of stress patterns from different implant-abutment interfaces. *Int J Oral Maxillofac Implants*. 2009;24:781–789.

38. Asvanund P, Morgano SM. Photoelastic stress analysis of external versus internal implant-abutment connections. *J Prosthet Dent*. 2011;196: 266–271.

Downloaded from http://meridian.allenpress.com/joi/article-pdf/41/2/155/2035673/aaid-joi-d-12-00260.pdf by guest on 17 April 2024